

HESSIAN RECOVERY BASED FINITE ELEMENT METHODS FOR THE CAHN-HILLIARD EQUATION

MINQIANG XU*, HAILONG GUO[†], AND QINGSONG ZOU[‡]

Abstract. In this paper, we propose a novel recovery based finite element method for the Cahn-Hilliard equation. One distinguishing feature of the method is that we discretize the fourth-order differential operator in a standard C^0 linear finite elements space. Precisely, we first transform the fourth-order Cahn-Hilliard equation to its variational formulation in which only first-order and second-order derivatives are involved and then we compute the first and second-order derivatives of a linear finite element function by a least-square-fitting recovery procedure. When the underlying mesh is uniform of regular pattern, our recovery scheme for the Laplacian operator coincides with the well-known five-point stencil. Another feature of the method is some special treatments on Neumann type boundary conditions for reducing computational cost. The optimal-order convergence properties and energy stability are numerically proved through a series of benchmark tests. The proposed method can be regarded as a combination of the finite difference scheme and the finite element scheme.

AMS subject classifications. Primary 65N30; Secondary 45N08

Key words. Hessian recovery, Cahn-Hilliard equation, phase separation, recovery based, superconvergence, linear finite element.

1. Introduction. The phase field model is a powerful tool to characterize interfacial problems in which the dynamics of the physical systems are described by a gradient flow. The Cahn-Hilliard equation [7] is a famous phase field model introduced by Cahn and Hilliard to model the phase separation in binary alloys. Later on, it is widely used to model multiphase flow [4, 11], tumor growth [36, 41], and image inpainting [5] etc.

As a nonlinear parabolic type equation, the analytic solution of the Cahn-Hilliard equation is usually hard to be obtained. Numerical simulation looks like to be the only feasible way to study the physical problems governed by the Cahn-Hilliard equation. During the past several decades, a huge number of numerical methods have been developed in the literature, including finite different methods [8], spectral methods [38], and finite element methods [18, 40, 43]. In this paper, we concentrate on finite element methods for the Cahn-Hilliard equation.

One of the main difficulties in the numerical solution of the Cahn-Hilliard equation is the discretization of the fourth-order differential operator in a certain finite element space. In the literature, finite element methods for fourth-order elliptic equations can be roughly categorized into the following four classes: conforming finite element methods [6, 12], nonconforming finite element methods [33], mixed finite element methods [13], discontinuous Galerkin method [20]. In corresponding, the Cahn-Hilliard equation has been numerically solved by conforming finite element methods in [15, 19], nonconforming finite element methods in [16, 43], mixed finite element methods in [17, 22], and discontinuous Galerkin methods [40, 42]. All the above methods in the primary form discretize the Cahn-Hilliard equation at least in a quadratic

*School of Data and Computer Science, Sun Yat-sen University, Guangzhou 510275, China (xumq9@mail2.sysu.edu.cn).

[†]School of Mathematics and Statistics, The University of Melbourne, Parkville, VIC 3010, Australia (hailong.guo@unimelb.edu.au).

[‡] School of Data and Computer Science and Guangdong Province Key Laboratory of Computational Science, Sun Yat-sen University, Guangzhou 510275, China (mcszqs@mail.sysu.edu.cn)

finite element space, which means that there are at least six degrees of freedom on each triangular element. To reduce the complexity, a new class of finite element methods, called recovery based finite element methods [10, 25, 28], is proposed to simulate fourth-order partial differential equations. The key idea of those methods is to facilitate the simplest element, the continuous linear element, to discretize the fourth-order differential operator. It is known that the second-order derivative of C^0 piecewise linear function is not well-defined and thus usually we can not solve a fourth-order differential equation in a C^0 linear finite element space. Such a barrier is alleviated by using the classical gradient recovery operator G_h [44, 46] to smooth the discontinuous piecewise constant function into a continuous piecewise linear function i [10, 25].

In this paper, we will also discretize the Cahn-Hilliard equation only in the simplest linear element space. Comparing to the recovery-based FEMs in [10, 25, 28], the difference here is that we directly recover the Hessian matrix of a linear finite element function instead of recovering its gradient. Note that the Hessian recovery has been studied for the purpose of post-processing [1, 23, 37, 39]. In particular, in [23], Guo et al. proposed a new Hessian recovery method and established its complete super-convergence theory on mildly unstructured meshes and ultraconvergence theory on structured meshes. The Hessian recovery technique in [23] is then applied to solving a sixth-order PDE in [26]. In this paper, we use a Hessian recovery technique by firstly recovering a local quadratic polynomial and then taking second order derivatives of the recovered polynomial as the *second-order derivatives* of the linear finite element function. We sprucely discover that there is an intrinsic connection between the Hessian recovery method and the finite difference method. In specific, we find that the Hessian recovery method reproduces the standard five-point finite difference scheme on regular pattern uniform meshes. This means, on the regular pattern uniform meshes, the new recovery based finite element method is a kind of infusion of the finite difference method and the finite element method in the sense that we first use the standard five-point finite difference scheme to discretize the Laplacian operator and then put it back into the standard linear finite element framework.

Different from second-order elliptic equations, the Neumann boundary condition for fourth-order partial differential equations is an essential boundary condition in the sense that the boundary condition should be enforced in their associate solution spaces. But it looks like impossible to be enforced into a C^0 linear finite element space. In our previous paper [10, 25, 26], it is imposed by the penalty method [14, 45] and the Lagrange multiplier method [3]. Like it for the second order partial differential equations, the resulting linear system of the penalty method is usually ill-conditioned. The Lagrange multiplier method shows the potential to overcome such drawback but it introduces additional degrees of freedom. In this paper, we adopt two different methods to deal with the Neumann boundary condition. On general unstructured meshes, we propose to impose the boundary condition weakly based on a technique called Nitsche's method [35], which is originally introduced by Nitsche to incorporate the Dirichlet boundary condition for second order elliptic equations. A Nitsche's variational formulation for the Cahn-Hilliard equations is presented. It paves the way for implicitly imposing the Neumann boundary conditions in Hessian recovery based finite element methods. As mentioned in the previous paragraph, the Hessian recovery method reduces to the standard five-point standard finite difference scheme on uniform meshes. Such key observation enables us to incorporate the Neumann boundary condition into the Hessian recovery operator by the celebrated ghost point

method in finite difference methods [29].

The rest of paper is organized as follows: In Section 2, we present a simple introduction to the Cahn-Hilliard equation and review some of its property. In Section 3, we first revisit the Hessian recovery method and uncover its relationship with the classical finite difference method; then, we propose the new recovery based finite element method to discretize the spatial variable; the fully discrete formulation is discussed through an energy stable time stepping method. The proposed method is numerically verified and validated using a series of benchmark examples in Section 4. We end with some conclusive remarks in Section 5.

2. The Cahn-Hilliard equation and its variational formulations. Let Ω be a bounded polygonal domain with Lipschitz boundary $\partial\Omega$ in \mathbb{R}^2 . For a subdomain \mathcal{A} of Ω , let $\mathbb{P}_m(\mathcal{A})$ be the space of polynomials of degree less than or equal to m over \mathcal{A} and n_m be the dimension of $\mathbb{P}_m(\mathcal{A})$ with $n_m = \frac{1}{2}(m+1)(m+2)$. We denote by $H^k(\mathcal{A})$ the Sobolev space with norm $\|\cdot\|_{k,\mathcal{A}}$ and seminorm $|\cdot|_{k,\mathcal{A}}$.

The well-known Cahn-Hilliard equation on a space domain Ω and a certain time period $[0, T]$ can be described as below:

$$\begin{cases} \frac{\partial u}{\partial t} = -\varepsilon^2 \Delta^2 u + \Delta F'(u), & \text{in } \Omega \times [0, T], \\ \partial_{\mathbf{n}} u = \partial_{\mathbf{n}}(-\varepsilon^2 \Delta u + F'(u)) = 0, & \text{on } \partial\Omega \times [0, T], \\ u(\cdot, 0) = u_0(\cdot), & \text{in } \Omega, \end{cases} \quad (2.1)$$

where \mathbf{n} is the unit outer normal vector of $\partial\Omega$. The unknown function u often indicates the concentration of one of the two metal components constituting the alloys, ε is the size of the interface of two alloys, F is a double well nonconvex function defined as $F(u) = \frac{1}{4}(u^2 - 1)^2$.

The Cahn-Hilliard equation (2.1) can be viewed as an H^{-1} -gradient flow of the Ginzburg-Landau free energy functional

$$E(u) := \int_{\Omega} \left(\frac{\varepsilon^2}{2} |\nabla u|^2 + F(u) \right) dx, \quad (2.2)$$

of which the first part is called the *interfacial energy* and the second part is called the *bulk energy*. Thanks to the homogeneous Neumann boundary conditions, it is easy to verify that the mass conservation property

$$\frac{d}{dt} \int_{\Omega} u dx = 0,$$

and the energy decay property

$$\frac{dE(u)}{dt} = -\| -\varepsilon^2 \Delta u + F'(u) \|^2 \leq 0, \quad \forall t > 0,$$

always hold for the solution of the Cahn-Hilliard equation.

Let $f = F'$. To implicitly impose the Neumann boundary condition $\partial_{\mathbf{n}} u = 0$, we introduce the bilinear form

$$a_1(w, v) = \int_{\Omega} \Delta w \Delta v dz - \int_{\partial\Omega} \Delta w \partial_{\mathbf{n}} v ds - \int_{\partial\Omega} \partial_{\mathbf{n}} w \Delta v ds + \gamma \int_{\partial\Omega} \partial_{\mathbf{n}} w \partial_{\mathbf{n}} v ds, \quad \forall v, w \in H^2(\Omega), \quad (2.3)$$

with γ is a positive stability parameter to be specified in the sequel. It is easy to verify that if $u \in H^2(\Omega)$ is the solution of (2.1), then u satisfies

$$\left(\frac{\partial u}{\partial t}, v \right) + \varepsilon^2 a_1(u, v) + (\nabla f(u), \nabla v) = 0, \quad \forall v \in H^2(\Omega). \quad (2.4)$$

Conversely, if $u \in C^4(\Omega)$ and $u_t \in C(\Omega)$ which satisfies (2.4), then for all $v \in H^2(\Omega)$, we have

$$\begin{aligned} & \left(\frac{\partial u}{\partial t} + \varepsilon^2 \Delta^2 u - \Delta f(u), v \right) \\ & - \int_{\partial\Omega} \partial_{\mathbf{n}} u \Delta v ds + \gamma \int_{\partial\Omega} \partial_{\mathbf{n}} u \partial_{\mathbf{n}} v + \int_{\partial\Omega} \partial_{\mathbf{n}} (-\varepsilon^2 \Delta u + F'(u)) v ds = 0. \end{aligned} \quad (2.5)$$

Choosing $v \in C_0^\infty(\Omega)$ in (2.5), we obtain

$$\left(\frac{\partial u}{\partial t} + \varepsilon^2 \Delta^2 u - \Delta f(u), v \right) = 0.$$

which implies $\frac{\partial u}{\partial t} + \varepsilon^2 \Delta^2 u - \Delta f(u) = 0$. Consequently, (2.5) becomes

$$- \int_{\partial\Omega} \partial_{\mathbf{n}} u \Delta v ds + \gamma \int_{\partial\Omega} \partial_{\mathbf{n}} u \partial_{\mathbf{n}} v + \int_{\partial\Omega} \partial_{\mathbf{n}} (-\varepsilon^2 \Delta u + f(u)) v ds = 0, v \in H^2(\Omega).$$

Since $v \in H^2(\Omega)$ is arbitrary, we derive from the above equation that

$$\partial_{\mathbf{n}} u = \partial_{\mathbf{n}} (-\varepsilon^2 \Delta u + f(u)) = 0$$

It means u is the classical solution of (2.1). From the above reasonings, we obtain that the solution of (2.4) is a weak solution of (2.1) and we call (2.4) a variational formulation of (2.1).

REMARK 2.1. *An alternative variational equation of (2.1) is*

$$\left(\frac{\partial u}{\partial t}, v \right) + \varepsilon^2 a_2(u, v) + (\nabla f(u), \nabla v) = 0, \quad \forall v \in H^2(\Omega) \quad (2.6)$$

where

$$a_2(w, v) = \int_{\Omega} D^2 w : D^2 v dx - \int_{\partial\Omega} \partial_{\mathbf{n}}^2 w \partial_{\mathbf{n}} v ds - \int_{\partial\Omega} \partial_{\mathbf{n}} w \partial_{\mathbf{n}}^2 v ds + \gamma \int_{\partial\Omega} \partial_{\mathbf{n}} w \partial_{\mathbf{n}} v ds, \quad (2.7)$$

and $A : B$ is the Frobenius norm of 2×2 matrices. We observe that here, the bilinear form $a_2(\cdot, \cdot)$ differs from $a_1(\cdot, \cdot)$ by replacing the Laplace operator Δ with the Hessian matrix operator D^2 .

In both variational formulations, the Neumann boundary conditions $\partial_{\mathbf{n}} u = 0$ is weakly built into the bilinear formations. The idea is similar to impose the Dirichlet boundary condition for the second-order elliptic equations by Nitsche [35]. We call those two methods the Nitsche's method.

REMARK 2.2. *Originally, the Neumann boundary condition for fourth-order partial differential equations is enforced into their solution space. For such purpose, let*

$$V = \{v \in H^2(\Omega) : \partial_{\mathbf{n}} v = 0 \text{ on } \partial\Omega\}. \quad (2.8)$$

The bilinear forms a_1 and a_2 in V reduce to

$$a_3(w, v) = \int_{\Omega} \Delta w \Delta v dx, w, v \in V \quad (2.9)$$

and

$$a_4(w, v) = \int_{\Omega} D^2 w : D^2 v dx, w, v \in V \quad (2.10)$$

respectively. Correspondingly, the variational formulations become to find $u \in (L^2([0, T]; V))$ such that

$$\left(\frac{\partial u}{\partial t}, v \right) + \varepsilon^2 a_3(u, v) + (\nabla f(u), \nabla v) = 0, \quad \forall v \in V, \quad (2.11)$$

or, to find $u \in (L^2([0, T]; V))$ such that

$$\left(\frac{\partial u}{\partial t}, v \right) + \varepsilon^2 a_4(u, v) + (\nabla f(u), \nabla v) = 0, \quad \forall v \in V. \quad (2.12)$$

3. A novel recovery based finite element method. In this section, we design novel recovery-technique-based finite element methods for Cahn-Hilliard equations. Since our main attention is on novel space discretization techniques, for the time discretization, we choose a simple one-step energy stable linear scheme proposed in [27, 38, 43]. Precisely, we make use of a semi-implicit scheme with an extra stabilized penalty term added to ensure energy stability. Let the time step size be $\Delta t = \frac{T}{N}$, $u^0(x) = u(x, 0)$, and $u^n(x) \approx u(x, n\Delta t)$, $n = 1, 2, \dots, N$, then the stabilized first-order semi-implicit method reads as: find $u^n \in S$, $n = 1, 2, \dots, N$ such that for all $v \in S$,

$$\begin{aligned} & \left(\frac{u^{n+1} - u^n}{\Delta t}, v \right) + \varepsilon^2 a_i(u^{n+1}, v) \\ & + (\nabla f(u^n), \nabla v) + \kappa (\nabla(u^{n+1} - u^n), \nabla v) = 0, \quad i = 1, 2, 3, 4, \end{aligned} \quad (3.1)$$

where $S = H^2(\Omega)$ for $i = 1, 2$ and $S = V$ for $i = 3, 4$. Note that the choice of κ has a great influence on the stability of (3.1), see [30, 32, 38, 43] for the details. In this paper, we always take $\kappa = 2$. In fact, [30, 32] give you rigorous analysis on the choose of κ .

Next we explain how to discretize (3.1) in a linear finite element space. Let \mathcal{T}_h be a shape regular *triangulation* of Ω with mesh size h . The set of all vertices and of all edges of \mathcal{T}_h are denoted by \mathcal{N}_h and \mathcal{E}_h , respectively. We define the standard continuous linear finite element space S_h on \mathcal{T}_h by

$$S_h := \{v_h \in C^0(\Omega) : v_h|_T \in \mathbb{P}_1, \forall T \in \mathcal{T}_h\}. \quad (3.2)$$

and denote its nodal basis by $\{\phi_z\}_{z \in \mathcal{N}_h}$.

To construct our fully discrete schemes on the linear finite element space S_h , we first introduce a Hessian recovery technique based on least-squares fitting in the first subsection. Then we apply the Hessian recovery operator to develop our novel fully discrete schemes for the Cahn-Hilliard equation in the second subsection.

3.1. A Hessian recovery operator in linear finite element spaces. It is known that the second order derivative of a function $v_h \in S_h$ equals to 0 in the interior of each element $T \in \mathcal{T}_h$ and is not well-defined on an edge $E \in \mathcal{E}_h$. In the following, we propose a *least-square type* method to calculate the *approximate second order derivatives* of v_h . In other words, we will define a *Hessian recovery operator* H_h from S_h to S_h^4 which maps a function $v_h \in S_h$ to $H_h v_h \in S_h^4$ so that $H_h v_h$ can be regarded as an approximation of the Hessian matrix of v_h in some sense.

Since $H_h v_h \in S_h^4$, to define $H_h v_h$, it is sufficient to define the value $(H_h v_h)(z)$ for all $z \in \mathcal{N}_h$. For this purpose, we first construct a local *patch* associated with z

which is a polygon surrounding the node z . Given a vertex $z \in \mathcal{N}_h$ and a nonnegative integer $n \in \mathbb{N}$, let the first n layer element patch be

$$\mathcal{L}(z, n) = \begin{cases} \{z\}, & \text{if } n = 0, \\ \bigcup\{T : T \in \mathcal{T}_h, \overline{T} \cap \mathcal{L}(z, 0) \neq \emptyset\}, & \text{if } n = 1, \\ \bigcup\{T : T \in \mathcal{T}_h, \overline{T} \cap \overline{\mathcal{L}(z, n-1)} \text{ is an edge in } \mathcal{E}_h\}, & \text{if } n \geq 2. \end{cases} \quad (3.3)$$

For all $z \in \mathcal{N}_h$, let n_z be the smallest integer such that $\mathcal{L}(z, n)$ satisfies the rank condition in the following sense.

DEFINITION 3.1. *A surrounding z polygon is said to satisfy the rank condition if it admits a unique least-squares fitted polynomial p_z in (3.4).*

We define the local patch associated with z as $\Omega_z = \mathbf{L}(z, n_z)$. Using the vertices in Ω_z as sampling points, we fit a quadratic polynomial p_z at the vertex z in the following least-squares sense

$$p_z = \arg \min_{p \in \mathbb{P}^2(\Omega_z)} \sum_{x \in \Omega_z \cap \mathcal{N}_h} |p(x) - v_h(x)|^2. \quad (3.4)$$

Then, we define the recovered Hessian node value by

$$(H_h v_h)(z) = \begin{pmatrix} H_h^{xx} v_h(z) & H_h^{xy} v_h(z) \\ H_h^{yx} v_h(z) & H_h^{yy} v_h(z) \end{pmatrix} = \begin{pmatrix} \frac{\partial^2 p_z}{\partial x^2}(z) & \frac{\partial^2 p_z}{\partial x \partial y}(z) \\ \frac{\partial^2 p_z}{\partial y \partial x}(z) & \frac{\partial^2 p_z}{\partial y^2}(z) \end{pmatrix}. \quad (3.5)$$

With this definition, we have $H_h v_h = \sum_{z \in \mathcal{N}_h} H_h v_h(z) \phi_z$ and the symmetric property $H_h^{xy} = H_h^{yx}$ of the Hessian matrix function $H_h v_h$. Moreover, based on H_h , we define a discrete Laplacian operator $\Delta_h : S_h \rightarrow S_h$ as

$$\Delta_h v_h = H_h^{xx} v_h + H_h^{yy} v_h. \quad (3.6)$$

Note that in the same way, we can recover the *gradient* of v_h by letting

$$(G_h v_h)(z) = \nabla p_z(z), \forall z \in \mathcal{N}_h \quad (3.7)$$

and $G_h v_h = \sum_{z \in \mathcal{N}_h} G_h v_h(z) \phi_z \in S_h^2$.

Note that the Hessian recovery operator H_h in (3.5) has been applied to post-process the finite element solution in [23]. According to the numerical results, sometimes it might be inefficient or even not convergent as a post-processing operator. Since it involves a relatively smaller number of neighbourhood vertices in its stencil, here we choose it as our pre-processing operator. In fact, H_h can be regarded as a special finite difference operator of the second order on uniform meshes and of the first order on general unstructured meshes. To elucidate this basic idea, we consider a special case that \mathcal{T}_h is a regular pattern uniform triangular mesh. In this case, for an interior node $z = z_i$, the local patch Ω_{z_i} is defined as the polygon $z_1 \cdots z_6$, see Figure 3.1a and thus the sampling points in Ω_{z_i} include $z_{i_0}, z_{i_1}, \dots, z_{i_6}$ with $z_{i_0} = z_i$. Using these seven sampling points, we fit a quadratic polynomial p_{z_i} in the least-squares sense and take second-order differentiation, which produces

$$\begin{aligned} (H_h^{xx} u)(z_i) &= \frac{1}{h^2} (u_1 - 2u_0 + u_4), \\ (H_h^{xy} u)(z_i) &= \frac{1}{2h^2} (2u_0 - u_1 + u_2 - u_3 - u_4 + u_5 - u_6), \\ (H_h^{yy} u)(z_i) &= \frac{1}{h^2} (u_3 - 2u_0 + u_6); \end{aligned}$$

where the values u_j is defined by $u_j = u(z_{i_j})$. By the definition of the discrete Laplacian operator (3.6), we have

$$(\Delta_h u)(z_i) = \frac{1}{h^2}(u_1 + u_3 - 4u_0 + u_4 + u_6). \quad (3.8)$$

The formula (3.8) implies the discrete Laplacian operator on regular pattern uniform meshes is the well-known five-point-finite-difference stencil of the Laplace operator, as illustrated in Figure 3.1b. By the standard approximation theory, we have

$$\|\Delta u - \Delta_h u_I\|_{0,\Omega} \leq Ch^2 \|u\|_{4,\Omega}. \quad (3.9)$$

This exciting discovery implies that the Hessian recovery operator can be regarded as an extension of the classic second-order difference operator on regular meshes to the difference operator on non-uniform meshes and thus it can be used to design discrete schemes for higher-order differential equations.

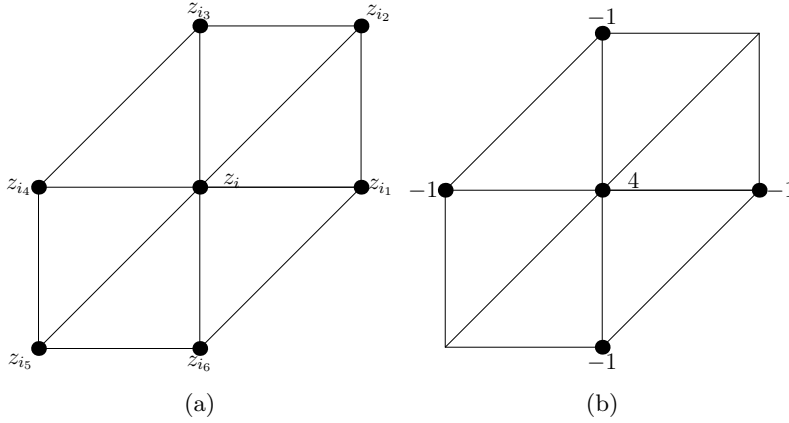


Fig. 3.1: Illustration of Hessian recovery on uniform mesh: (a) local patch ; (b) Discrete Laplace operator.

REMARK 3.1. For a boundary vertex $z \in \partial\Omega$, there are other approaches to construct the local patch Ω_z , see [24] for the details.

3.2. Fully discrete schemes. To present our fully discrete schemes, we first introduce the discrete bilinear form $a_{i,h}(\cdot, \cdot)$ on the linear finite element space S_h . For all $w_h, v_h \in S_h$, we define

$$\begin{aligned} a_{1,h}(w_h, v_h) = & \int_{\Omega} \Delta_h w_h \Delta_h v_h dz - \int_{\partial\Omega} \Delta_h w_h (G_h v_h \cdot \mathbf{n}) ds \\ & - \int_{\partial\Omega} (G_h w_h \cdot \mathbf{n}) \Delta_h v_h ds + \gamma \int_{\partial\Omega} (G_h w_h \cdot \mathbf{n})(G_h v_h \cdot \mathbf{n}) ds, \end{aligned} \quad (3.10)$$

and

$$\begin{aligned} a_{2,h}(w_h, v_h) = & \int_{\Omega} H_h w_h H_h v_h dz - \int_{\partial\Omega} (\mathbf{n}^T H_h w_h \mathbf{n})(G_h v_h \cdot \mathbf{n}) ds \\ & - \int_{\partial\Omega} (G_h w_h \cdot \mathbf{n})(\mathbf{n}^T H_h v_h \mathbf{n}) ds + \gamma \int_{\partial\Omega} (G_h w_h \cdot \mathbf{n})(G_h v_h \cdot \mathbf{n}) ds, \end{aligned} \quad (3.11)$$

where $\gamma = \frac{C}{h}$ with C a sufficiently large positive constant.

The fully discrete Hessian recovery based finite element method for the Cahn-Hilliard equation (2.1) reads as : find $\{u_h^n\}_{n \geq 1} \in V_h$ such that for all $v_h \in S_h$,

$$\left(\frac{u_h^{n+1} - u_h^n}{\Delta t}, v_h \right) + \varepsilon^2 a_{i,h}(u_h^{n+1}, v_h) + \kappa(\nabla u_h^{n+1} - \nabla u_h^n, \nabla v_h) + (\nabla f(u_h^n), \nabla v_h) = 0. \quad (3.12)$$

Note that both the schemes in (3.12) work on general unstructured meshes. Moreover, our numerical experiments indicate that there is no essential difference between these two schemes. We also observe that the stiffness matrices corresponding to both schemes (3.12) are symmetric and positive definite, so both schemes are stable and uniquely solvable.

Next, we present a simple fully discrete scheme derived from the variational formulation (2.11) on uniform meshes. We define the finite element space $S_{h,0} \subset S_h$ as

$$S_{h,0} = \{v_h \in S_h : \nabla_h v_h(z) \cdot \mathbf{n} = 0, \forall z \in \mathcal{N}_h \cap \partial\Omega\}, \quad (3.13)$$

where ∇_h is a discrete gradient operator so that $S_{h,0}$ be a discrete analogous of V . Note that in the continuous linear finite element space S_h , $\nabla v_h \cdot \mathbf{n}$ is not well defined on a vertex of \mathcal{T}_h , so at each boundary vertex, we use a central finite difference scheme instead of $\nabla v_h(z)$ to define $\nabla_h v_h(z)$.

The key part in construction of a simpler scheme on the uniform meshes is based on the fact the discrete Laplacian operator Δ_h reduces to the five-point-finite-difference stencil at an interior vertex, as illustrated in (3.8). Now, we suppose Δ_h is the discrete Laplacian operator on the finite element space $S_{h,0}$. Different from the general treatment of the recovery on the boundary as introduced in the previous subsection, we borrow the idea of ghost point method from the finite difference method [29]. In specific, at every boundary vertex z_i , we introduce one or more ghost points. Then, we still have the fact that the the discrete Laplacian operator Δ_h is just the five-point finite difference stencil at the boundary vertex z_i but it involves the value of the finite element function at the ghost points. To eliminate it, we combine the discrete boundary condition $\nabla_h v_h(z_i) \cdot \mathbf{n} = 0$ which also involves the same ghost points.

To illustrate idea, we consider a typical boundary vertex z_i , as illustrated in Figure 3.2a. In that case, z_i is a boundary vertex with three neighbour mesh vertices $z_{i_1}, z_{i_2}, z_{i_3}$. To apply the five-point finite difference scheme at z_i , we introduce a ghost point z_{i_4} , as the red dot point in Figure 3.2a, and the discrete Laplacian $\Delta v_h(z_i)$ is

$$\Delta v_h(z_i) = \frac{1}{h^2} (v_h(z_{i_1}) + v_h(z_{i_2}) - 4v_h(z_i) + v_h(z_{i_3}) + v_h(z_{i_4})), \quad (3.14)$$

which involves the ghost point finite element function value $v_h(z_{i_4})$. By the definition of the finite element space $S_{h,0}$, at the boundary vertex z_i , we also

$$\nabla_h v_h(z_i) \cdot \mathbf{n} = \frac{1}{2h} (v_h(z_{i_4}) - v_h(z_{i_2})) = 0. \quad (3.15)$$

Using (3.14) and (3.15) to eliminate $v_h(z_{i_4})$, we obtain

$$\Delta v_h(z_i) = \frac{1}{h^2} (v_h(z_{i_1}) + 2v_h(z_{i_2}) - 4v_h(z_i) + v_h(z_{i_3})), \quad (3.16)$$

which only depends on the value at the vertices in \mathcal{N}_h . In other word, we have embedding the discrete Neumann boundary condition into the discrete Laplacian operator Δ_h . Similarly, we can explicitly construct the discrete Laplacian operator Δ_h at a corner boundary vertex, which may need two ghost points as plotted in Figure 3.2b. In this case, the computation of Δ_h does not need to use an implicit least-squares fitting process.

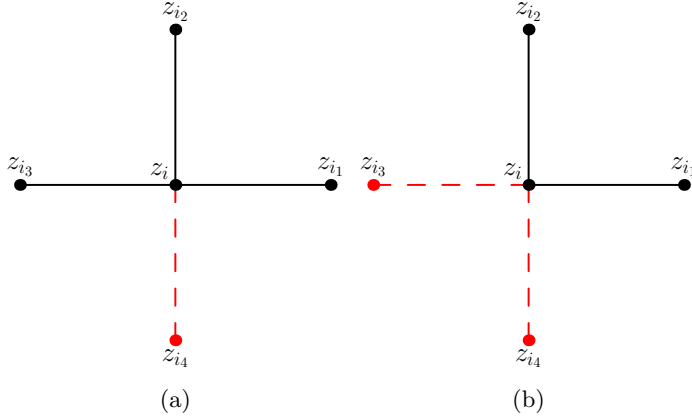


Fig. 3.2: Illustration of ghost point method: (a). One ghost point; (b) Two Ghost points.

REMARK 3.2. *The key processing is to build the discrete Neumann boundary condition into the discrete Laplacian operator Δ_h . Such process is only possible for the uniform meshes. For general unstructured meshes, we can define a similar discrete finite element space as $S_{h,0} = \{v_h \in S_h : G_h v_h(z_i) \cdot \mathbf{n} = 0, \forall z_i \in \mathcal{N}_h \cap \partial\Omega\}$. But the discrete boundary condition $G_h v_h(z_i) \cdot \mathbf{n} = 0$ can not be embedded into discrete Laplacian operator Δ_h . We have to use other methods like the penalty method [14, 45] and the Lagrange multiplier method [3] to impose the discrete Neumann boundary condition $G_h v_h(z_i) \cdot \mathbf{n} = 0, \forall z_i \in \mathcal{N}_h \cap \partial\Omega$. However, these two methods perform badly for the Cahn-Hilliard equation.*

Then the discrete bilinear $a_{3,h}(\cdot, \cdot)$ on $S_{h,0}$ as

$$a_{3,h}(w_h, v_h) = \int_{\Omega} \Delta_h w_h \Delta_h v_h dx, \quad \forall v_h, w_h \in S_{h,0}. \quad (3.17)$$

A simple fully discrete for (2.1) on uniform meshes is to find $\{u_h^n\}_{n \geq 1} \in S_{h,0}$ such that for all $v_h \in S_{h,0}$,

$$\left(\frac{u_h^{n+1} - u_h^n}{\Delta t}, v_h \right) + \varepsilon^2 a_{3,h}(u_h^{n+1}, v_h) + \kappa (\nabla u_h^{n+1} - \nabla u_h^n, \nabla v_h) + (\nabla f(u_h^n), \nabla v_h) = 0. \quad (3.18)$$

Since the bilinear form $a_{3,h}(\cdot, \cdot)$ does not involve the computation of the gradient recovery operator G_h either, the scheme (3.18) is very computationally efficient and accurate. Moreover, the scheme (3.18) can be regarded as a mixture of the finite difference method and the finite element method since we first use the finite difference operator Δ_h to recover the second order derivatives of a linear finite element function

and then bring them back to the framework of the finite element method. Namely, the scheme (3.18) sheds some light on using the finite difference operators to construct simple finite element methods for higher-order partial differential equations.

It may worth mentioning that the gradient recovered method proposed in [25] for fourth-order problems use the minimum number of degrees of freedom among the finite element spaces, see for details. However, our numerical experiments show that a direct application of the gradient recovered method to the Cahn-Hilliard equation leads to an unstable scheme. Moreover, compared with the gradient recovered method, the present Hessian recovered method uses the same number of total degree but its stiffness matrix is more sparse than the one derived from the gradient-recovered method.

4. Numerical Experiments. In this section, we present several numerical examples to demonstrate the properties of our proposed methods.

Except for the last numerical example, the domain Ω of the problems in this section is chosen as the unit square $[0, 1]^2$. In our experiments, we will adopt two different types of meshes: the uniform and unstructured meshes. Our uniform meshes are generated by first dividing Ω into m^2 congruent subsquares and then splitting each subsquare into two right-angled triangles, see Figure 4.1a. Our unstructured meshes are generated by the first partition of the domain with the Delaunay mesh generator *EasyMesh* [34] to obtain the first level mesh and then uniformly refines each triangle in the first level mesh several times, see Figure 4.1b. On a uniform mesh, we will use the fully discrete scheme (3.18), while on an unstructured mesh, we will use the scheme (3.12) with $i = 1, \kappa = 2, C = 1$ to solve numerically the Cahn-Hilliard equations.

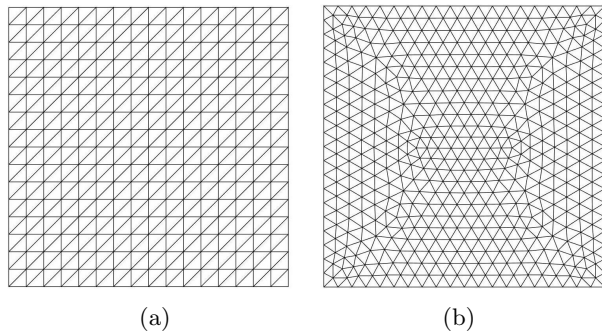


Fig. 4.1: (a) A uniform mesh; (b) An unstructured mesh.

Throughout this section, we define discrete interface energy and discrete buck energy at time t_n respectively as :

$$E_1^n = \frac{\epsilon^2}{2} \sum_{\tau \in \mathcal{T}_h} \int_{\tau} |G_h u_h^n|^2 dx dy, \quad E_2^n = \frac{1}{4} \sum_{\tau \in \mathcal{T}_h} \int_{\tau} ((u_h^n)^2 - 1)^2 dx dy.$$

Moreover, we denote different kinds of numerical errors by

$$e_0 = \|u - u_h\|_{0,\Omega}, \quad e_1 = \|\nabla u - \nabla u_h\|_{0,\Omega}, \\ e_{1,r} = \|\nabla u - G_h u_h\|_{0,\Omega}, \quad e_2 = \|D^2 u - H_h u_h\|_{0,\Omega},$$

and use $r = \frac{\log(\epsilon_h/\epsilon_{h/2})}{\log(2)}$ to indicate the convergence rates.

4.1. Accuracy. Example 1: We consider the non-homogeneous Cahn-Hilliard equation

$$\begin{cases} \frac{\partial u}{\partial t} = -\epsilon^2 \Delta^2 u + \Delta(u^3 - u) + g, & \text{in } \Omega \times [0, T], \\ \partial_{\mathbf{n}} u = \partial_{\mathbf{n}} \Delta u = 0, & \text{on } \partial\Omega \times [0, T], \end{cases} \quad (4.1)$$

with the parameter $\epsilon = 0.1$. The initial solution u_0 and g are chosen such that the exact solution is

$$u(x, y, t) = e^{-2t} \cos(\pi x) \cos(\pi y).$$

To compute the convergence rates with respect to the space meshsize h , we fix the time step size $\Delta t = 10^{-6}$ and study the convergence order of the numerical solution at $T = 0.1$ computed by the scheme (3.18) on uniform meshes and by the scheme (3.12) ($i = 1, C = 1, \kappa = 2$) on unstructured meshes. The numerical results by (3.18) and (3.12) are depicted in Table 4.1 and Table 4.2, respectively. From these two tables, we observe that for both schemes, the L^2 -norm errors converge with order 2 while the H^1 -seminorm errors converge with order 1 which are both optimal for a linear finite element method. We also observe that the recovered H^1 -seminorm error is superconvergent of $\mathcal{O}(h^2)$ while the recovered H^2 -seminorm errors converges optimally with order 1.

To test the convergence rate of the scheme (3.18) with respect to the time discretization, we fix the spacial mesh size $h = 1/128$. The corresponding numerical results at $T = 0.01$ with different time step Δt are shown in Table 4.3. The numerical results evidently indicate that the scheme (3.18) is of first order in time, which is consistent with the first-order semi-implicit scheme.

Table 4.1: *Spatial errors and convergence rates by scheme (3.18) for Example 1*

h	e_0	r	e_1	r	$e_{1,r}$	r	e_2	r
1/16	1.87×10^{-2}		2.46×10^{-1}		1.49×10^{-1}		2.78×10^{-0}	
1/32	4.09×10^{-3}	2.2	9.65×10^{-1}	1.4	2.99×10^{-2}	2.3	6.52×10^{-1}	1.9
1/64	9.92×10^{-4}	2.0	4.55×10^{-2}	1.1	7.47×10^{-3}	2.0	2.98×10^{-1}	1.3
1/128	2.47×10^{-4}	2.0	2.24×10^{-2}	1.0	1.87×10^{-3}	2.0	1.39×10^{-1}	1.1
1/256	6.14×10^{-5}	2.0	1.12×10^{-2}	1.0	4.67×10^{-4}	2.0	6.86×10^{-2}	1.0

Table 4.2: *Spatial errors and convergence rates by scheme (3.12) for Example 1*

dof	e_0	r	e_1	r	$e_{1,r}$	r	e_2	r
513	1.20×10^{-2}		1.61×10^{-1}		8.77×10^{-2}		2.31×10^{-0}	
1969	2.45×10^{-3}	2.3	5.64×10^{-2}	1.5	1.66×10^{-2}	2.4	1.10×10^{-1}	1.1
7713	6.01×10^{-4}	2.0	2.59×10^{-2}	1.1	4.16×10^{-3}	2.0	5.37×10^{-1}	1.0
30529	1.52×10^{-4}	2.0	1.27×10^{-2}	1.0	1.08×10^{-3}	2.0	2.66×10^{-1}	1.0

Example 2: We consider the Cahn-Hilliard equation (2.1) with the parameter $\epsilon = 0.1$ and the initial value $u_0 = \cos(\pi x) \cos(\pi y)$.

We use the simple scheme (3.18) to compute the numerical results. As the exact solution of Example 2 is unknown, we use the computable quantity $u_{h/2} - u_h$ to replace the “true error” $e = u - u_h$ in our real computations. As in the previous example,

Table 4.3: *Temporal errors and convergence rate by scheme (3.18) for Example 1*

Δt	10^{-3}	$10^{-3}/2$	$10^{-3}/2^2$	$10^{-3}/2^3$	r
e_0	1.13×10^{-3}	5.66×10^{-4}	2.83×10^{-4}	1.41×10^{-4}	1.0

we fix $\Delta t = 10^{-5}$ and $T = 0.1$ to test the convergence behaviour of the spatial discretization. The corresponding numerical errors and convergence rates are shown in Table 4.4. We can observe similar convergence and superconvergence results as in Example 1.

Also as in the previous example, we test the convergence rate of the time discretization by fixing $h = 1/128$ and $T = 0.01$. The numerical results with different time step Δt are presented in Table 4.5. We observe that the scheme (3.18) has a first-order accuracy in time discretization.

Table 4.4: *Spatial errors and convergence rates by scheme (3.18) for Example 2*

h	e_0	r	e_1	r	$e_{1,r}$	r	e_2	r
1/16	1.64×10^{-2}		5.23×10^{-1}		1.31×10^{-1}		4.94×10^{-0}	
1/32	3.59×10^{-3}	2.2	2.18×10^{-1}	1.3	2.62×10^{-2}	2.3	1.08×10^{-0}	2.2
1/64	8.71×10^{-4}	2.0	1.05×10^{-1}	1.1	6.55×10^{-3}	2.0	3.02×10^{-1}	1.9
1/128	2.16×10^{-4}	2.0	5.02×10^{-2}	1.1	1.64×10^{-3}	2.0	9.00×10^{-2}	1.8

Table 4.5: *Temporal errors and convergence rate by scheme (3.18) for Example 1*

Δt	10^{-4}	$10^{-4}/2$	$10^{-4}/2^2$	$10^{-4}/2^3$	r
e_0	1.80×10^{-4}	9.32×10^{-5}	4.72×10^{-5}	2.43×10^{-5}	1.0

4.2. Spinodal decomposition. In this subsection, we numerically solve the Cahn-Hilliard equation to show the spinodal decomposition: a process or phenomenon to rapidly unmix a mixture of liquids or solids from one thermodynamic phase, to form two coexisting phases. In the following examples, we apply the scheme (3.18) on the uniform triangular mesh with the space stepsize $h = 1/128$ and time stepsize $\Delta t = 10^{-3}$. Since the numerical results computed by the scheme (3.12) on unstructured meshes are similar to those by (3.18), they will be not reported here.

Example 3: We consider the Cahn-Hilliard equation suggested in [43] where the parameter $\epsilon = 0.02$ and the initial value is given by

$$u_0 = 10^{-3} \sin^3 \frac{\pi x}{4h} \sin^3 \frac{\pi y}{4h}, \quad (x, y) \in (0, 8h) \times (0, 8h).$$

We depict the phases at six different times in Fig. 4.2. Note that typical phase transition phenomena can be clearly observed from these pictures. Moreover, we find that under a small perturbation (u_0 is small near the origin), the spinodal decomposition occurs and then coarsens, and after a period of evolution, the two coexisting phases become stable. Note that, compared to the subsequent motion, the initial separation occurs over a very small time scale. Moreover, the evolution of the energies, including bulk energy and interfacial energy, is shown in Fig. 4.3a, the development of the mass is displayed in Fig. 4.3b, the maximum-norm of the numerical solution is illustrated in Fig. 4.3c. Apparently, the presented method almost preserves the

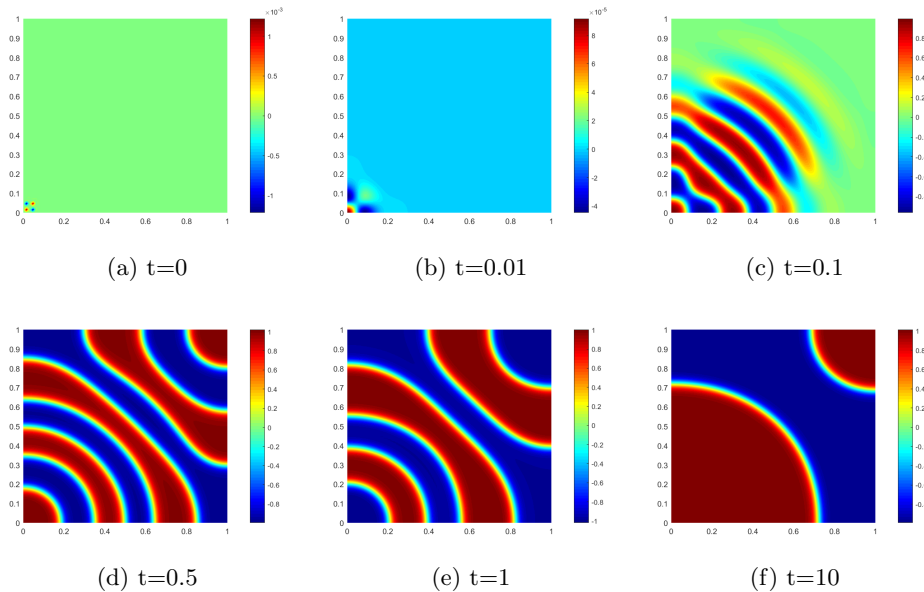


Fig. 4.2: Example 4, *spinoidal decomposition at six fixed time.*

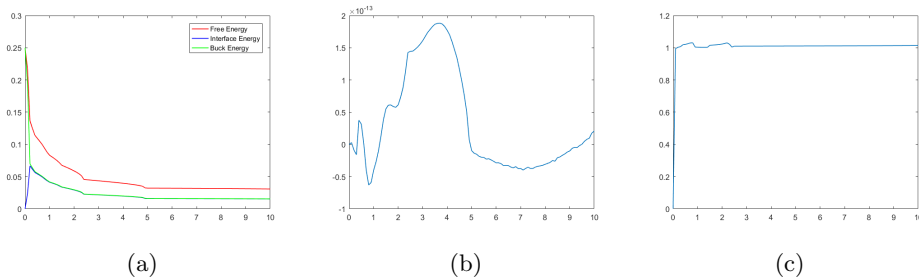


Fig. 4.3: Example 4 (a): *Energies evolution*, (b): *Mass evolution*, (c): *Evolution of the maximum-norm of the solution.*

properties of energy dissipation and mass conservation, while the numerical solution itself is uniformly bounded.

Example 4: We consider the Cahn-Hilliard equation suggested in [2] where the initial data u_0 is a random value field which is uniformly distributed between -1 and 1 . The parameter ϵ is set to be 0.02 . We depict the phase evolution of Example 4 in Fig.4.4. The process of phase evolution is similar to that in Example 3. That is, the spinodal decomposition takes place very early, and after a brief period of evolution, the separation becomes very slow. Fig. 4.4 is also in good agreement with the one presented in [2] by using the C^1 virtual element method. The discrete energies and mass are shown in Fig. 4.5a and Fig. 4.5b. The maximum norm of the approximate solution is displayed in Fig. 4.5c. These numerical results reveal that our numerical scheme is energy stable.

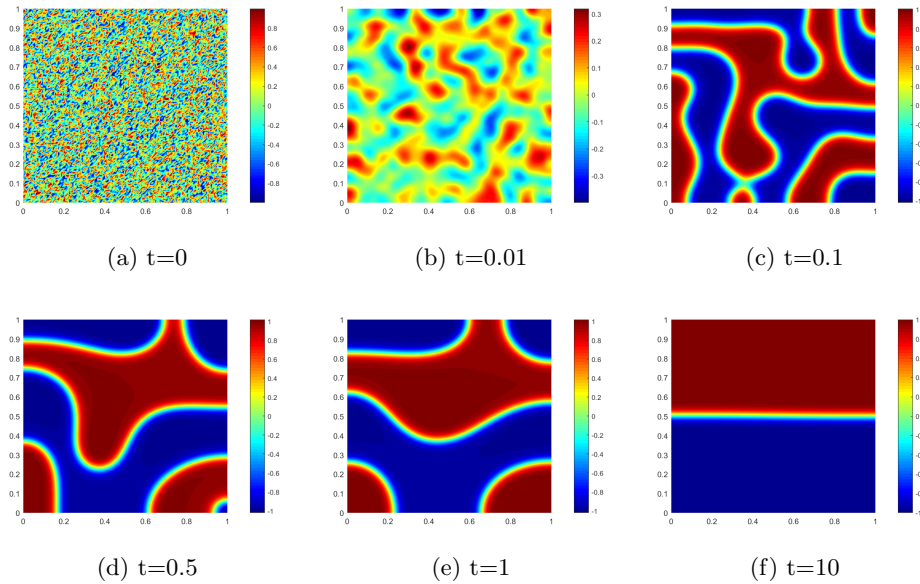


Fig. 4.4: Example 4, *spinoidal decomposition at six fixed time.*

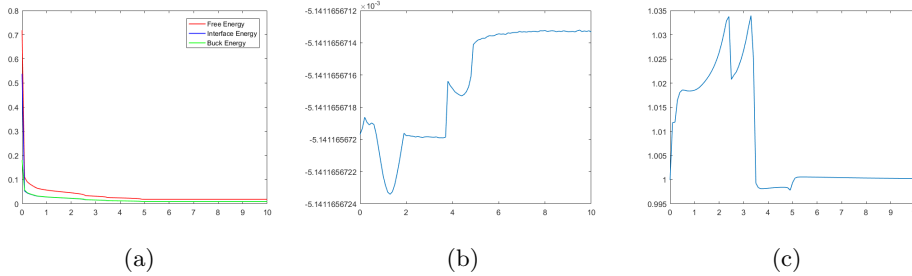


Fig. 4.5: Example 4 (a): *Energies evolution*, (b): *Mass evolution*, (c): *Evolution of the maximum-norm of the solution.*

4.3. Evolution of interfaces. In this subsection, we focus on tracking the evolution of initial data's interfaces, including a cross-shaped, an elliptic-shaped and two circles-shaped interfaces between phases. In all examples, we use the uniform mesh with mesh size $h = 1/128$ and time step size $\Delta t = 5 \times 10^{-5}$.

Example 5: We consider the Cahn-Hilliard equation suggested in [9] with $\epsilon = 0.01$ and the initial value

$$u_0(x, y) = \begin{cases} 0.95, & \text{if } 5|(y - 0.5) - (x - 0.5)| + |\frac{2}{5}(x - 0.5) - (y - 0.5)| < 1, \\ 0.95, & \text{if } 5|(x - 0.5) - (y - 0.5)| + |\frac{2}{5}(y - 0.5) - (x - 0.5)| < 1, \\ -0.95, & \text{otherwise.} \end{cases}$$

From Fig. 4.6, we observe that the cross-shaped interface evolves toward a steady circular interface. From Fig. 4.7, we observe that the mass is well preserved, the energy is dissipative and the maximum norm of the approximate solution is controlled.

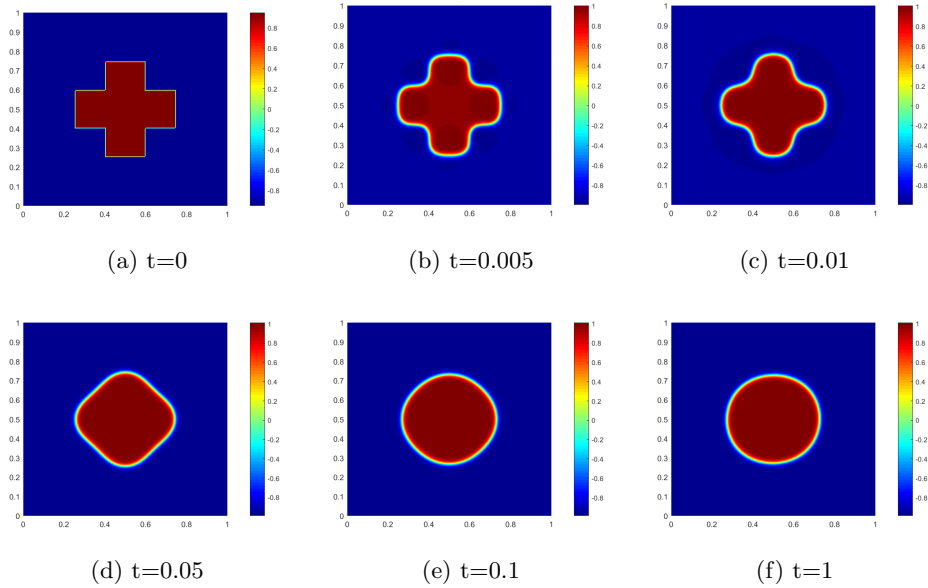


Fig. 4.6: Example 5 *Evolution of a cross-shaped interface at six temporal frames.*

Comparing Fig. 4.6 with the numerical results given in [9] computed by the mixed FEM, they are in good agreement.

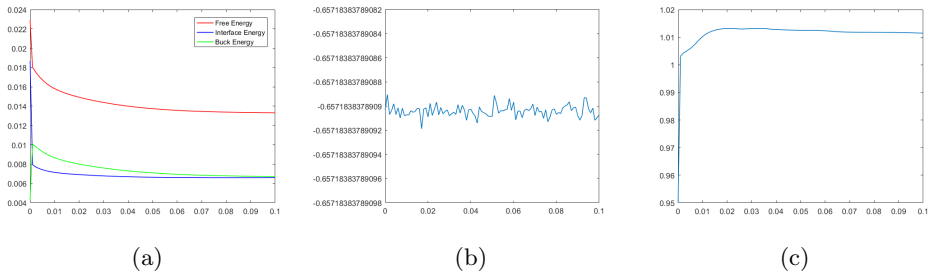


Fig. 4.7: Example 5 (a) *Energies evolution* (b) *Mass evolution*, (c) *Evolution of the maximum norm of the approximate solution.*

Example 6: We consider the Cahn-Hilliard equation with a piecewise constant initial data u_0 whose jump set has a shape of an ellipse:

$$u_0(x, y) = \begin{cases} 0.95, & \text{if } 81(x - 0.5)^2 + 9(y - 0.5)^2 < 1, \\ -0.95, & \text{otherwise.} \end{cases}$$

and the parameter is set to be $\epsilon = 0.01$.

The numerical results are presented in Fig. 4.8. As in the previous example, we found that the initial interface evolves to a steady state exhibiting a circular interface. Moreover, the features of the mass and energies are also captured, as shown in Fig. 4.9.

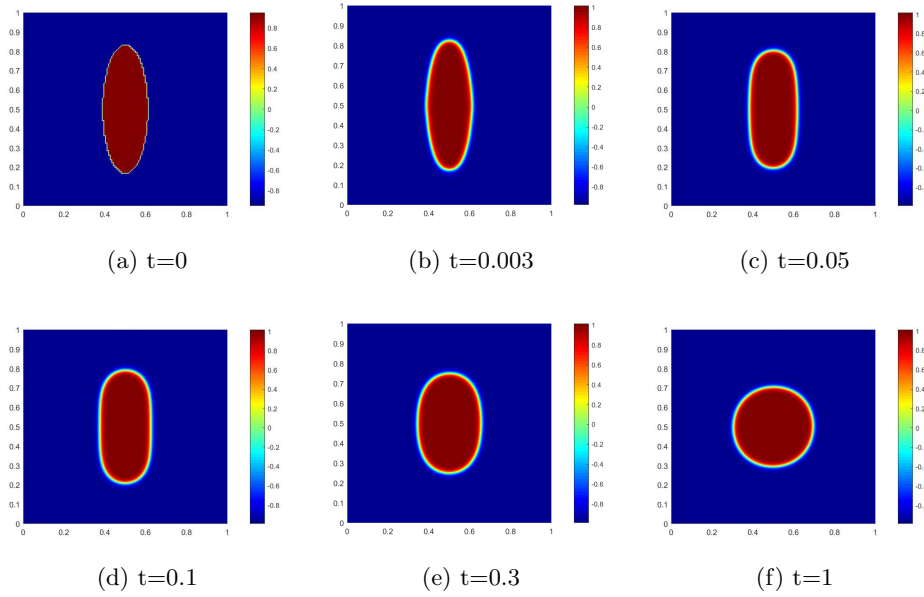


Fig. 4.8: Example 6 *Evolution of a cross-shaped interface at six temporal frames.*

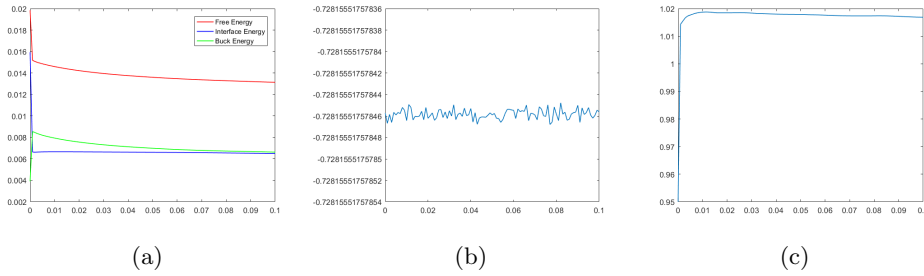


Fig. 4.9: Example 6 (a) *Energies evolution* (b) *Mass evolution*, (c) *Evolution of the maximum norm of the approximate solution.*

Example 7: We consider the Cahn-Hilliard equation with $\epsilon = 0.025$ on the domain $[-1, 1]^2$ and the initial value

$$u_0(x) = \tanh\left(\frac{1}{\sqrt{2}\epsilon} \min\{\sqrt{(x+0.3)^2 + y^2} - 0.3, \sqrt{(x-0.3)^2 + y^2} - 0.25\}\right).$$

We generate six snapshots at six fixed time points in Fig. 4.10. This graph clearly indicates that the two circle interfaces gradually evolve into one circle, which is consistent with the maximum-norm results obtained in [21]. Numerical results depicting the mass, energies and solution's evolution are shown in Fig. 4.11.

5. Conclusion. We designed a C^0 linear finite element method to solve the Cahn-Hilliard equations. This method has a minimum total degree of freedoms and is very simple in implementation. A series of numerical examples indicate that the new

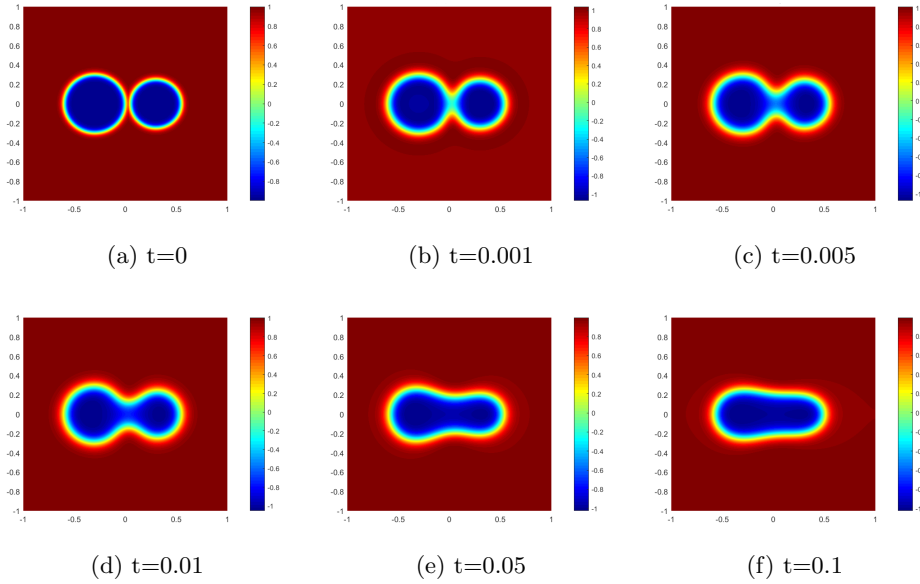


Fig. 4.10: Example 7 *Evolution of a cross-shaped interface at six temporal frames.*

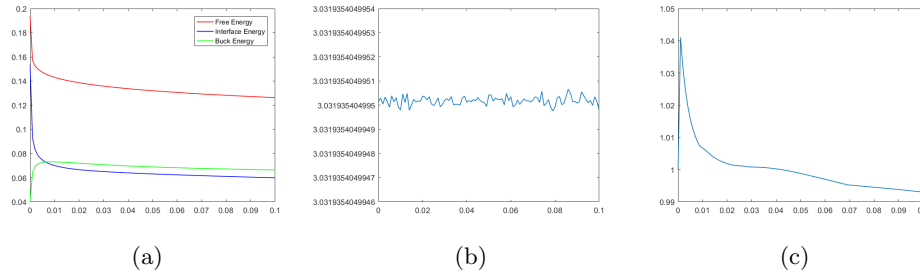


Fig. 4.11: Example 7 (a) *Energies evolution* (b) *Mass evolution*, (c) *Evolution of the maximum norm of the approximate solution.*

method is stable, efficient and is able to capture some important physical features such as energy decay and mass conservation during the phase evolution process governed by the Cahn-Hilliard equations. Meanwhile, the numerical results reveal that our novel method has the optimal convergence orders.

Ongoing research topics include a theoretical analysis of the proposed method and an extension of the presented method to 3D Cahn-Hilliard equations and/or other high order differential equations. For 3D Cahn-Hilliard equation, we adopt similar stabilization method [31] for time discretization.

REFERENCES

- [1] A. AGOUZAL AND Y. VASSILEVSKI, *On a discrete Hessian recovery for P_1 finite elements*, J. Numer. Math., 10 (2002), pp. 1–12.
- [2] P. F. ANTONIETTI, L. BEIRÃO DA VEIGA, S. SCACCHI, AND M. VERANI, *A C^1 virtual element method for the Cahn-Hilliard equation with polygonal meshes*, SIAM J. Numer. Anal., 54 (2016), pp. 34–56.
- [3] I. BABUŠKA, *The finite element method with Lagrangian multipliers*, Numer. Math., 20 (1972/73), pp. 179–192.
- [4] V. E. BADALASSI, H. D. CENICEROS, AND S. BANERJEE, *Computation of multiphase systems with phase field models*, J. Comput. Phys., 190 (2003), pp. 371–397.
- [5] ANDREA L. BERTOZZI, SELIM ESEDOLU, AND ALAN GILLETTE, *Inpainting of binary images using the Cahn-Hilliard equation*, IEEE Trans. Image Process., 16 (2007), pp. 285–291.
- [6] S. C. BRENNER AND L. R. SCOTT, *The mathematical theory of finite element methods*, vol. 15 of Texts in Applied Mathematics, Springer, New York, third ed., 2008.
- [7] JOHN W CAHN AND JOHN E HILLIARD, *Free energy of a nonuniform system. i. interfacial free energy*, The Journal of Chemical Physics, 28 (1958), p. 258.
- [8] H. D. CENICEROS AND A. M. ROMA, *A nonstiff, adaptive mesh refinement-based method for the Cahn-Hilliard equation*, J. Comput. Phys., 225 (2007), pp. 1849–1862.
- [9] F. CHAVE, D. A. DI PIETRO, F. MARCHE, AND F. PIGEONNEAU, *A hybrid high-order method for the Cahn-Hilliard problem in mixed form*, SIAM J. Numer. Anal., 54 (2016), pp. 1873–1898.
- [10] H. CHEN, H. GUO, Z. ZHANG, AND Q. ZOU, *A C^0 linear finite element method for two fourth-order eigenvalue problems*, IMA J. Numer. Anal., 37 (2017), pp. 2120–2138.
- [11] Y. CHEN AND J. SHEN, *Efficient, adaptive energy stable schemes for the incompressible Cahn-Hilliard Navier-Stokes phase-field models*, J. Comput. Phys., 308 (2016), pp. 40–56.
- [12] P. G. CIARLET, *The finite element method for elliptic problems*, vol. 40 of Classics in Applied Mathematics, Society for Industrial and Applied Mathematics (SIAM), Philadelphia, PA, 2002. Reprint of the 1978 original [North-Holland, Amsterdam; MR0520174 (58 #25001)].
- [13] P. G. CIARLET AND P.-A. RAVIART, *A mixed finite element method for the biharmonic equation*, (1974), pp. 125–145. Publication No. 33.
- [14] R. COURANT, *Variational methods for the solution of problems of equilibrium and vibrations*, Bull. Amer. Math. Soc., 49 (1943), pp. 1–23.
- [15] Q. DU AND R. A. NICOLAIDES, *Numerical analysis of a continuum model of phase transition*, SIAM J. Numer. Anal., 28 (1991), pp. 1310–1322.
- [16] C. M. ELLIOTT AND D. A. FRENCH, *A nonconforming finite-element method for the two-dimensional Cahn-Hilliard equation*, SIAM J. Numer. Anal., 26 (1989), pp. 884–903.
- [17] C. M. ELLIOTT, D. A. FRENCH, AND F. A. MILNER, *A second order splitting method for the Cahn-Hilliard equation*, Numer. Math., 54 (1989), pp. 575–590.
- [18] C. M. ELLIOTT AND S. LARSSON, *Error estimates with smooth and nonsmooth data for a finite element method for the Cahn-Hilliard equation*, Math. Comp., 58 (1992), pp. 603–630, S33–S36.
- [19] C. M. ELLIOTT AND S. ZHENG, *On the Cahn-Hilliard equation*, Arch. Rational Mech. Anal., 96 (1986), pp. 339–357.
- [20] G. ENGEL, K. GARIKIPATI, T. J. R. HUGHES, M. G. LARSON, L. MAZZEI, AND R. L. TAYLOR, *Continuous/discontinuous finite element approximations of fourth-order elliptic problems in structural and continuum mechanics with applications to thin beams and plates, and strain gradient elasticity*, Comput. Methods Appl. Mech. Engrg., 191 (2002), pp. 3669–3750.
- [21] X. FENG, Y. LI, AND Y. XING, *Analysis of mixed interior penalty discontinuous Galerkin methods for the Cahn-Hilliard equation and the Hele-Shaw flow*, SIAM J. Numer. Anal., 54 (2016), pp. 825–847.
- [22] X. FENG AND A. PROHL, *Error analysis of a mixed finite element method for the Cahn-Hilliard equation*, Numer. Math., 99 (2004), pp. 47–84.
- [23] H. GUO, Z. ZHANG, AND R. ZHAO, *Hessian recovery for finite element methods*, Math. Comp., 86 (2017), pp. 1671–1692.
- [24] H. GUO, Z. ZHANG, R. ZHAO, AND Q. ZOU, *Polynomial preserving recovery on boundary*, J. Comput. Appl. Math., 307 (2016), pp. 119–133.
- [25] H. GUO, Z. ZHANG, AND Q. ZOU, *A C^0 linear finite element method for biharmonic problems*, J. Sci. Comput., 74 (2018), pp. 1397–1422.
- [26] ———, *A C^0 linear finite element method for sixth order elliptic equations*, 2018. arXiv:1804.03793v2.
- [27] Y. HE, Y. LIU, AND T. TANG, *On large time-stepping methods for the Cahn-Hilliard equation*, Appl. Numer. Math., 57 (2007), pp. 616–628.
- [28] B. P. LAMICHHANE, *A finite element method for a biharmonic equation based on gradient*

- recovery operators, BIT, 54 (2014), pp. 469–484.
- [29] R. J. LEVEQUE, *Finite difference methods for ordinary and partial differential equations*, Society for Industrial and Applied Mathematics (SIAM), Philadelphia, PA, 2007. Steady-state and time-dependent problems.
 - [30] D. LI AND Z. QIAO, *On second order semi-implicit Fourier spectral methods for 2D Cahn-Hilliard equations*, J. Sci. Comput., 70 (2017), pp. 301–341.
 - [31] ———, *On the stabilization size of semi-implicit Fourier-spectral methods for 3D Cahn-Hilliard equations*, Commun. Math. Sci., 15 (2017), pp. 1489–1506.
 - [32] D. LI, Z. QIAO, AND T. TANG, *Characterizing the stabilization size for semi-implicit Fourier-spectral method to phase field equations*, SIAM J. Numer. Anal., 54 (2016), pp. 1653–1681.
 - [33] L. S. D MORLEY, *The triangular equilibrium element in the solution of plate bending problems*, Aerosp. Quart., 19 (1968), pp. 149–169.
 - [34] B. NICENO, *EasyMesh: A two-dimensional quality mesh generator*. http://web.mit.edu/easymesh_v1.4/www/easymesh.html, 2001.
 - [35] J. NITSCHKE, *über ein Variationsprinzip zur Lösung von Dirichlet-Problemen bei Verwendung von Teilräumen, die keinen Randbedingungen unterworfen sind*, Abh. Math. Sem. Univ. Hamburg, 36 (1971), pp. 9–15. Collection of articles dedicated to Lothar Collatz on his sixtieth birthday.
 - [36] J. T. ODEN, A. HAWKINS, AND S. PRUDHOMME, *General diffuse-interface theories and an approach to predictive tumor growth modeling*, Math. Models Methods Appl. Sci., 20 (2010), pp. 477–517.
 - [37] M. PICASSO, F. ALAUZET, H. BOROCHAKI, AND P.-L. GEORGE, *A numerical study of some Hessian recovery techniques on isotropic and anisotropic meshes*, SIAM J. Sci. Comput., 33 (2011), pp. 1058–1076.
 - [38] J. SHEN AND X. YANG, *Numerical approximations of Allen-Cahn and Cahn-Hilliard equations*, Discrete Contin. Dyn. Syst., 28 (2010), pp. 1669–1691.
 - [39] M.-G. VALLET, C.-M. MANOLE, J. DOMPIERRE, S. DUFOUR, AND F. GUIBAULT, *Numerical comparison of some Hessian recovery techniques*, Internat. J. Numer. Methods Engrg., 72 (2007), pp. 987–1007.
 - [40] G. N. WELLS, E. KUHL, AND K. GARIKIPATI, *A discontinuous Galerkin method for the Cahn-Hilliard equation*, J. Comput. Phys., 218 (2006), pp. 860–877.
 - [41] S. M. WISE, J. S. LOWENGRUB, H. B. FRIEBOES, AND V. CRISTINI, *Three-dimensional multi-species nonlinear tumor growth—I: Model and numerical method*, J. Theoret. Biol., 253 (2008), pp. 524–543.
 - [42] Y. XIA, Y. XU, AND C.-W. SHU, *Local discontinuous Galerkin methods for the Cahn-Hilliard type equations*, J. Comput. Phys., 227 (2007), pp. 472–491.
 - [43] S. ZHANG AND M. WANG, *A nonconforming finite element method for the Cahn-Hilliard equation*, J. Comput. Phys., 229 (2010), pp. 7361–7372.
 - [44] Z. ZHANG AND A. NAGA, *A new finite element gradient recovery method: superconvergence property*, SIAM J. Sci. Comput., 26 (2005), pp. 1192–1213 (electronic).
 - [45] O. C. ZIENKIEWICZ, R. L. TAYLOR, AND J. Z. ZHU, *The finite element method: its basis and fundamentals*, Elsevier/Butterworth Heinemann, Amsterdam, seventh ed., 2013.
 - [46] O. C. ZIENKIEWICZ AND J. Z. ZHU, *The superconvergent patch recovery and a posteriori error estimates. I. The recovery technique*, Internat. J. Numer. Methods Engrg., 33 (1992), pp. 1331–1364.